SINGLE AND DOUBLE BRACEWELL NULLING INTERFEROMETER IN SPACE

T. Velusamy[(1)], R.P. Angel[(2)], A. Eatchel[(2)], D. Tenerelli[(3)], N.J. Woolf[(2)]

[(1)]Jet Propulsion Laboratory (Caltech), 4800 Oak Grove Drive, Pasadena, CA 91109, USA,
E-mail: Thangasamy.Velusamy@jpl.nasa.gov
[(2)]University of Arizona, Steward Observatory, 933 N. Cherry, Tucson, Az 85721, USA
[(3)]Lockheed Martin Missiles and Space, 1111 Lockheed Martin Way, Sunnyvale, CA 94089, USA

ABSTRACT

As part of a NASA NRA study we have examined the design and use of a small Bracewell nulling interferometer in space for observations of Jovian and terrestrial planets in the 4-12 μm spectral region. At these wavelengths, the contrast is typically 10^{-7} for most planets while younger and/or more massive Jovian planets have a contrast 100 times better. For planets farther from their star than Earth, a short baseline can provide good null depth and still have adequate resolution. With the single Bracewell nulling interferometer described here, massive/young giant planets far from their star are not difficult to observe and young Jovian mass planetary systems as far as 100 pc can be probed. A program to study planetary systems like the solar system is much harder. In the case of older and smaller planets, distinguishing the planet signal from the star and local zodiacal background is much harder and requires both high stability of the gain for the IR detectors, and nulling over periods of hours. The difficulties of a 2-telescope, single Bracewell nuller are overcome using a dual Bracewell nuller consisting of four telescopes, and phase chopping between two null beams. Double Bracewell nulling described here will have the potential to detect Earth's around 20 nearby stars.

1. INTRODUCTION

NASA's Terrestrial Planet Finder (TPF) mission mainly aims at the direct detection and atmospheric characterization of Earth-like planets orbiting in the habitable zone of nearby (within ≈20 pc) main sequence stars. The corresponding requirements in terms of angular resolution (up to 50 mas), sensitivity and dynamical range (from typically 10^6 in the infrared to 10^9 in the visible) make it an extraordinarily challenging task. A space borne precursor with somewhat reduced scientific objectives, proving nulling and passive cooling in Earth-trailing orbit appears as a mandatory step to prepare for a full TPF mission. The direct observation of extrasolar terrestrial planets is far more difficult than studying the young self-luminous extrasolar Jupiters.

The progress in TPF requires smaller steps in which technology development and science are carried out on less expensive missions. The University of Arizona, Lockheed, and JPL have carried out a design and performance study of the simplest version of an IR nulling interferometer in space consisting of two 1-2 m diameter telescopes, with 8–18 m baseline on a boom, operating at 5–10 μm. While such a system is far below the needs of TPF, it is a viable mission to detect and characterize hot Jupiters in young planetary systems. The Jupiters ($M > 1\ M_J$) in young planetary systems (age < 1 Gyr) are warm, self-luminous and orbiting at any large distance from their star can be seen in thermal emission (especially at 5 μm). The IR interferometer will have the sensitivity and resolution at 5 μm to detect Jupiters in the young clusters, over a wide range of ages, from 8 Myr (Eta Cam at 100 pc) to 650 Myr (Hyades at 45 pc). The technologies for the structural, thermal, and the optics design are well understood and are being tested. A simple two telescope Bracewell interferometer will have high signal to noise ratio (SNR) for the young Jupiters. However, in spite of the fact that exo-earths in nearby stars will have sufficient SNR, detecting Earths has serious limitations mitigating systematic effects such as stellar leakage and background signal levels in the interferometer output. We discuss a modest design change to provide a dual Bracewell nulling which will be more robust to achieve the science goals, including the prospects for detecting Earths in a small sample of nearby stars.

2. SINGLE BRACEWELL NULLING INTERFEROMETER

The classical detection scheme to be used with a space-based infrared nulling interferometer is described by Bracewell and MacPhie[1]. A 2-telescope nulling interferometer (Fig. 1) is the simplest nulling configuration and when it is properly phased it produces a dark fringe on the line of sight. This would enable planet detection by suppressing starlight by pointing a null in the interference fringe pattern on the star. As the fringe pattern rotates over the sky, an off-axis source (planet) appears to successively cross regions of bright and dark fringes and its signal gets correspondingly modulated (Fig. 4). On the other hand, the central star is kept on axis (i.e., constantly nulled). Planets are localized through the characteristic intensity modulations observed as the interferometer rotates. However, the output is contaminated by unwanted signals, such as the leakage of the

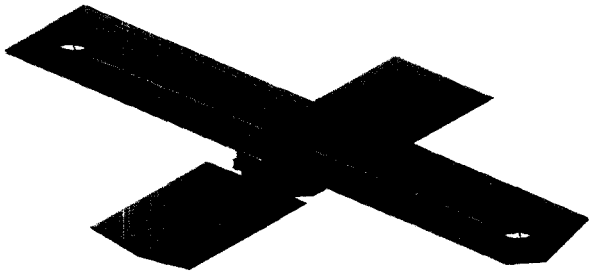

Fig. 1a. A space-based IR nulling interferometer.

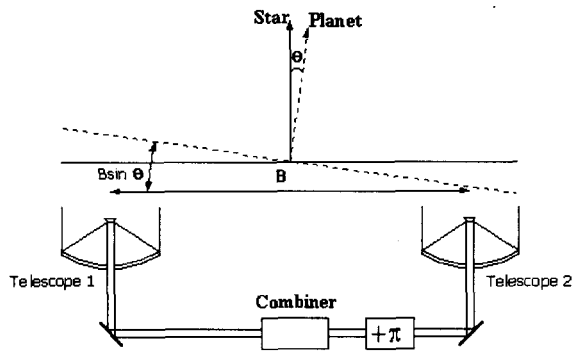

Fig. 1b. A two-element nulling interferometer.

Table 1. Parameters used for Single Bracewell

Baseline (B) 18 m	Aperture diameter 2 m
Efficiency 0.1	OPD Error:
Null Depth 3×10^{-5}	5.4 nm (5 μm)
T_{tel} 60 K	10.6 nm (10 μm)
T_{opt} 17 K	Spectral Resolution 3
$T_{detector}$ 7K	Integration 24 hr

starlight through the null and the exo-zodi (EZ) emission, and background emissions from the local-zodi (LZ) and the telescope system. Ultimately these signals, contributing to the output intensity and noise, limit the planet detection.

The beams from the two telescopes are co-axially recombined with appropriate internal achromatic phase shift π in one of the interferometer beams, to achieve destructive interference in the direction of the star (on a zero optical path difference (OPD) sky direction) [2]. Planets around the star exhibit an additional external OPD and their light is not nulled. The monochromatic intensity distribution in the final focal plane of a nulling interferometer (transmission response) is given by

$$P(\theta,\alpha) \sim \sin^2\phi \qquad (1)$$

$$\phi = 2\pi\mathbf{B}\cdot\mathbf{S}/2\lambda = (2\pi\theta B/2\lambda)\cos(\beta-\alpha) \qquad (2)$$

where **B** is the baseline vector and **S** is the line of sight of the off-axis sky position (x, y) or (θ, α). β and α are

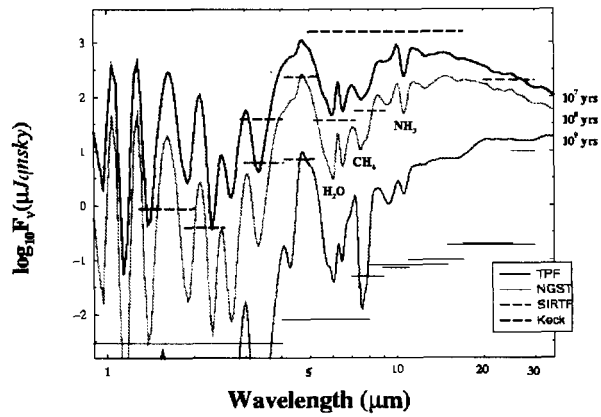

Fig. 2. Flux densities at 10pc of a Jupiter mass planet are shown for 3 ages of the planet [4].

position angles of the baseline and the source, and θ is the angular distance of source from the meridian plane of the interferometer. The interferometer projects a nulling interference pattern onto the sky whose response decreases as $\sim \theta^2$ near the null. A θ^2 null response is spatially broad enough to fill the stellar disk at a depth < 10^{-5} only for short baselines. However, a short baseline will produce broad fringes, limiting the angular resolution. For planets > 1AU from a star, a short baseline can provide good null depth (the interferometer does not appreciably resolve the stellar disk) and still have adequate resolution (planet appearing beyond the first fringe maximum).

3. YOUNG PLANETARY SYSTEMS

Radial velocity surveys have led to groundbreaking discoveries of Jupiter-mass planets around nearby solar type stars [3]. However, this method becomes less efficient for planet searches around young stars with active atmospheres, and stars of spectral type earlier than F7, stars that tend to have fewer spectral lines, and those are rotationally broadened. On the other hand, young massive planets are self-luminous for a long time and well suited for detection of their IR emission. Even at the age of the solar system, Jupiter and Saturn are mainly self-luminous in the IR. Younger and more massive planets are overwhelmingly self-luminous. Giant planet self-luminosity shows up most distinctly at 5μm, where there is a hole in giant planet atmospheric opacity [4]. Furthermore, at this wavelength neither local nor exo-zodi emission will limit the observations. In Fig. 2, the flux densities of a young Jupiter mass planet are shown.

Direct imagery of giant planets tells us about their mass and age. Young Jupiters are warm. In the IR they can be seen to any orbital distance from the star. Single Bracewell has the resolution and sensitivity for young planetary systems in a number star clusters (Table 2).

Table 2. Candidate sources of stars

Group	Age (years)	Distance (pc)
Eta Cam.	8×10^6	100
TW Hya	1×10^7	50
Upper Scorpius	1×10^7	140
IC2391 Super Cluster	5×10^7	175
Pleiades	1.2×10^8	125
Ursa Major stream	3×10^8	25
Hyades	6.5×10^8	45

The best candidates are the younger moving groups of stars. We need to study a variety of ages, as shown in Table-2. Such a sample studied with the IR nulling interferometry will provide important information in at least three general areas of extrasolar planetary science:

1. The dynamical structure of newly formed planetary systems to retain terrestrial planets in habitable zones
2. The origin of diversity among extrasolar planets
3. The evolution of multiple planetary systems.

A systematic search for planetary systems around young stars in clusters, association, and star forming regions out to a distance of 100 pc can provide valuable information on the formation mechanisms of gaseous giant planets: How does the initial planet mass function change with mass of primary star? How does the planet mass change with distance from the star? What fraction of outer planets is lost after formation? - (a) inside star clusters (b) outside star clusters.

Formation of giant planets through gas accretion is preceded by coagulation of planetesimals into several earth-mass cores [5]. In this scenario, terrestrial planets are the failed cores. Thus the presence of Jupiter- mass gaseous giant planets may be regarded as signposts where terrestrial planets may be formed.

4. PLANETARY DETECTION WITH SINGLE BRACEWELL INTERFEROMETER

4.1 Signal Levels and Noise

To simulate the nulling interferometer data realistically, we must take into consideration all sources of both signal and noise in an observation. A variety of sources contribute to the interferometer output, some relating to the target system, some to the instrument and its location in space [6]:

- Size, temperature and atmospheric composition of the target planet
- Distance to the star, the luminosity and physical size of the star
- Exo-zodi dust in the target star and the inclination of the orbital plane to the line of sight
- Observatory properties such as the size and temperature of the telescopes, and associated optics, interferometer baseline, pointing jitter, etc.

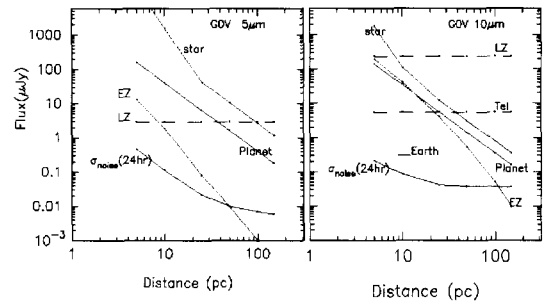

Fig. 3. Signal levels as a function of distance to the star.

- Instrument properties such as optical efficiencies, detector dark current, depth and stability of the null.
- Background due to the LZ at the interferometer location in space and in the direction of the target.

Each of these factors was evaluated using the parameters in Table 1, for a wide range of planetary and stellar targets and distances. Fig. 3 shows the signal and noise levels in the interferometer output at 5 and 10 μm as a function of the distance to the star. The signals and rms noise were simulated for G0V star at distances of 3 to 150 pc. The planet flux was assumed to be that of a Jupiter mass giant planet at an age of 0.5 Gyr (which is also equivalent to that of a planet with $M_p = 5\ M_J$ at the age of 1 Gyr). The rms noise corresponds to 24 hr integration. At 5 μm the star leak is the dominant signal in the output and this scales approximately as the planet flux with distance. On the other hand at 10 μm the local-zodi is the dominant signal and it is independent of the distance to the star. As a result, the ratio of planet signal to rms noise decreases more rapidly with increasing star distance at 10 μm than at 5 μm, making planet detection more efficient at 5 μm. Although the Earth flux density at 10 μm is well above the rms noise level (Fig. 3), it is 3 – 4 orders of magnitude below the other signals, making the detection very difficult.

Planets are detected by their characteristic intensity modulation with the rotation of the baseline as the planets move in and out of the dark and bright fringes. In Fig. 4 is shown an example of the simulated output showing the characteristic planet signal modulation with rotation of the baseline. Note the high background level in the output. The signal to noise in the data is high enough for easy detection of the planet even when the planet is closer to the star, that is, inside the first fringe maximum. However for the cases when the planet separation from the star is greater than θ_{max} (the first fringe maximum) are likely to give robust solutions for planet fluxes and locations. The decrease in the amplitude of planet modulation for the cases when the planet is closer to the star than first fringe maximum makes it difficult for planet detection especially, if slow drifts in the background signal level are present.

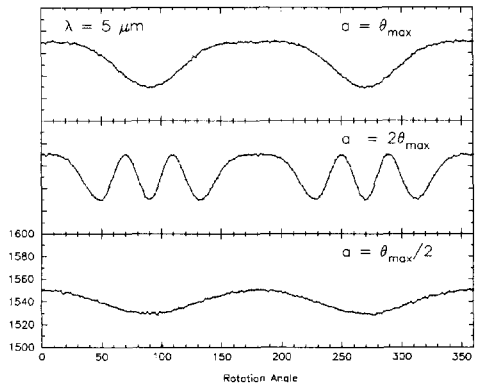

Fig. 4. Planet signal modulations in the 5μm output for a hot Jupiter (400K) at three distances from the star. First fringe maximum, θ_{max} is at 0.3 AU (at 10pc).

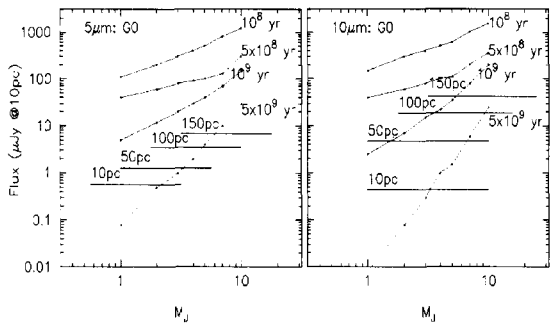

Fig. 5. Planet fluxes and detection limits at 5 and 10 μm.

4.2 Planetary Detection Limits

As seen in Fig. 4, the characteristic planet signal modulation is large enough for easy detection of the planet. We simulated data for a wide range of ages and masses for the giant planets and stars of spectral types from K0 to A0. We used flux densities given by the models for giant planets [4]. The detection limits (SNR = 5) are summarized in Fig. 5 as a function of planet mass, age and distance for a G0 star. The horizontal lines represent the limiting fluxes for detection at the indicated distances. Fig. 6 summarizes the detection limits as a function of star distance for spectral types K0 - A0.

The simulations show that in the case of G stars, giant planet detection is complete for distances up to 100 pc for planet masses > 1 M_J with ages < 1 Gyr and at orbit distance (a) > 3 AU. Older (5 Gyr) Jupiter mass planets are below the detection limit. However more massive (5 M_J) and older (5 Gyr) planets are still detectable for distances up to 100 pc in all spectral types except A0. For the 5 μm angular resolution of the interferometer, the detection limit for closest orbit distance increases from 0.3 AU for stars at 10 pc to 3 AU at 100 pc. Orbital motion at 20 AU around the star is still measurable with a 2.5 – 5 yr mission. For younger stars and clusters (age < 100 Myr) the distance limit for planet detection increases to larger distances. At 5 μm, the interferometer will have sensitivity and resolution to detect Jupiter

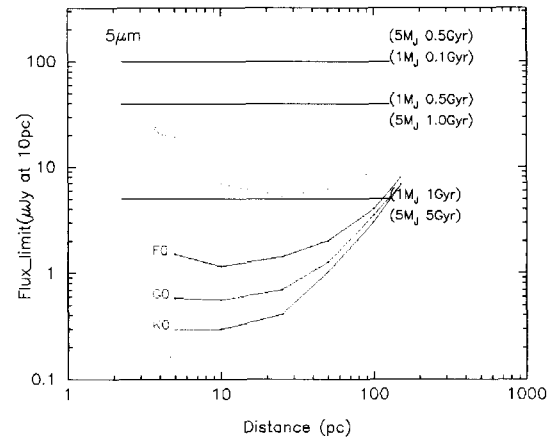

Fig. 6. Detection limits for K0, G0, F0, A0 stars. The flux levels for mass/age of the giant planets are shown.

mass giant planets with orbital distance > 5 AU around stars in Pleiades (120 Myr) at 125 pc and in Scorpius (10 Myr) at 140 pc.

As shown in Fig. 4, the background level in the output is high compared to the modulating planet signal. Any drifts in this background level will make it difficult to separate the planet signal from star leakage, local zodi, etc. Discriminating the modulating planet signal places stringent stability requirements on the sources of background signals such as optics thermal emission, local zodiacal light and residual stellar emission, as well as on detector quantum efficiency, dark current, and amplifier gain over long periods (typically 6-8 hrs, for one rotation of the baseline). This means that background subtraction of the order of one part in 10^4 is required for Earth detection (Fig. 3). However, the young giant planets are so self-luminous that background subtraction at a level of a few percent would be enough. It does not seem realistic to assume that background levels will remain constant even at the few percent levels for period of hours. Some kind of chopping appears mandatory to allow proper background drift subtractions.

Spatial chopping at a frequency of up to 10^3 Hz between the on axis star and an off-axis direction located a few arcsecs away will possibly eliminate most background fluctuations. With this chopping scheme, stellar leak fluctuations remain. Its implementation is difficult, as it would interrupt star and fringe tracking. Indeed one would like a scheme where the star should be kept nulled while chopping. Implementation of spatial chopping is under investigation. A more robust chopping scheme (e.g., Double Bracewell) requires the use of at least two sub-nulling interferometers, introducing a time variable phase shift between the different nulled output beams prior to detection [7] [8]. This scheme allows the removal of fluctuations of both background and the residual stellar flux. Nevertheless it is very complex to

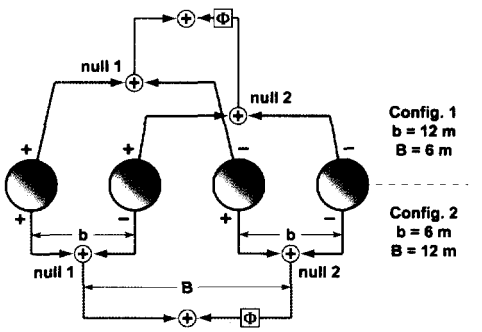

Fig. 7. Schematic of Double Bracewell.

implement: it requires more telescopes, and an additional cross-combiner stage providing accurate variable and ideally achromatic phase shifts. For science goals limited to self-luminous giant planets, a spatial chop would be adequate. However for Earth detection, a dual null beam chopper like a double Bracewell will be required.

5. DOUBLE BRACEWELL

A double Bracewell allows phase chop between two null beams, providing robust output in which the contributions from the stellar leakage, LZ, EZ, etc. are significantly reduced.

Fig. 7 shows a schematic of a double Bracewell IR interferometer consisting of a 4-telescope array on a fixed boom of 18 m. The beam combination allows two choices for the baseline (b) of the nulling elements to be 12 m/6 m and baseline (B) between the phase centers of the nulling elements to be 6 m/12 m, respectively. Two null beams are combined with a time varying phase shift Φ introduced in one of the null beams. Thus the null response pattern in the sky is changed in accordance with the phase shift introduced, while the star is still being kept in the null. The chopping between phases $\Phi = \pm \pi/2$ produces a sin-chop response, while chopping between $\Phi = (0, \pi)$ produces a cos-chop response.

In Fig. 8, the response patterns produced by sin- and cos- chops in a double Bracewell (config. 2) are compared with that of a single Bracewell for the parameters given in Fig. 7 and Table 1. The sin-chop is more attractive because of its asymmetrical response, and it significantly reduces any extended symmetrical structures (EZ) present around the star. This feature enhances the ability to discriminate planet signal from the EZ signal and thus makes Earth observing possible. The leakage of the star through the nulls is also subtracted out along with the other background signals. However, the star leakage, EZ and all other background signals do contribute to the photon noise in the detector outputs before the chop, that is, for each setting of the phase shift, Φ.

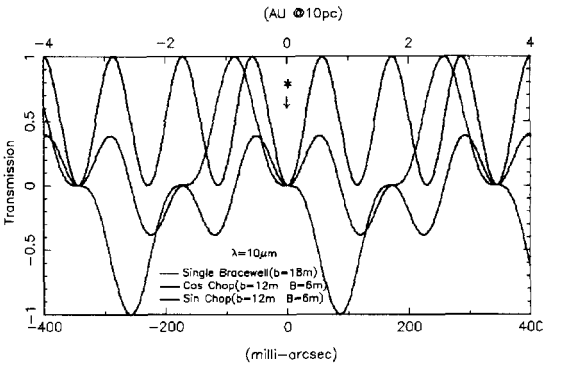

Fig. 8. Responses for single and double Bracewell sin- and cos- chops.

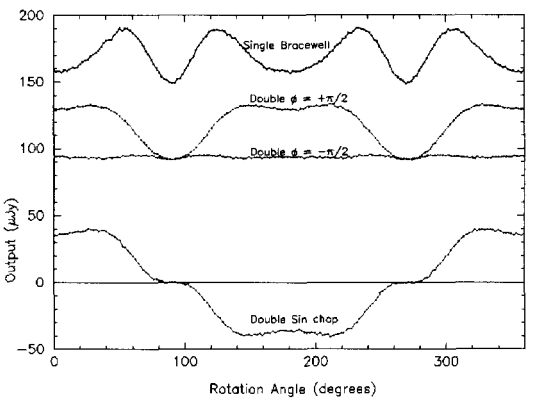

Fig. 9. Comparison of signal levels in single and double Bracewell.

Fig. 9 shows a comparison of the simulated signal levels for sin-chop in a double Bracewell. A giant planet with 5 μm flux of 40 μJy (corresponding to 1 M_J and age 0.5 Gyr) in a 1AU orbit around a G0 star at 10 pc. In contrast to the single Bracewell, in the case of sin-chop the planet signal modulation, occurring on a zero background level, can be easily detected. Thus exo-earth detections are feasible with a double Bracewell.

6. IMAGING PLANETARY SYSTEMS

Images of planetary systems are not formed by direct imaging. Instead, these images are reconstructed after measurements have been made with the interferometer in multiple orientations and configurations. The Fourier transform technique is commonly used in aperture synthesis. However in the nulling interferometers, the complex visibility measurement is precluded by the need for destructive interference on the star. Images can still be recovered from the measured intensities, at different orientations of the baseline, by a cross correlation method. The Maximum Correlation Method (MCM) reconstructs the image recursively, starting with an initial image uniformly sampled in a rectilinear grid in the image space. MCM constructs the image in a way that it

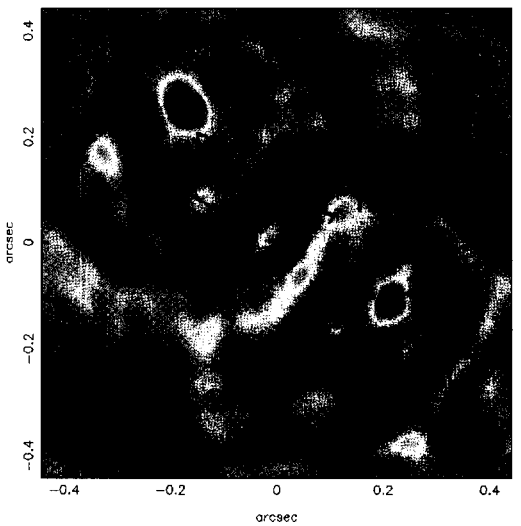

Fig. 10. MCM image reconstruction of a planetary system. Note the anti-symmetry of planet signals introduced by the sin-chop.

maintains the maximum pixel correlation consistent with the measurements and the null-response pattern [9]. Because of the lack of phase information and the signals that are completely symmetric about a 180° rotation of the baseline (Fig. 4), each point source appears twice in the reconstructed image, reflected through the central star. However in the case of double Bracewell with sin-chop, the interferometer response is asymmetric (Fig. 8) and the signals are anti-symmetric about a 180° rotation of the baseline (Fig. 9). Hence in the reconstructed image a point source will show an anti-symmetry about the star.

Fig. 10 shows an example of an image reconstructed using the double Bracewell sin-chop data for a planetary system. The simulations assumed 3 giant planets of age 0.5 Gyr and masses 1, 3, and 5 M_J orbiting at 1.5, 2.5 and 3.5 AU around a G0 star at 10 pc. The planets and their associated anti-symmetric peak locations are marked. The other low level features are artifacts caused by the limited number of baselines used. In special cases of a double Bracewell where the baselines B >> b (Fig. 7), use of both sin- and cos- chop signals provides a measure of complex visibility and a more robust imaging analogous to the Fourier transform method is possible [9].

7. PROSPECTS FOR EXO-EARTHS

A double Bracewell has a sensitivity $\sigma_{noise}(24hr) \approx$ 0.06 μJy, which is high enough to achieve a SNR ≈ 5 for Earth around a G0 star at 10 pc. Besides, as the exozodi is significantly resolved out by the sin-chop, separating planet signal and hence Earth detections are now feasible. It has the potential to detect Earths in about 20 nearby stars with 1-2 day integration. In Table 3, we list

Table 3. Exo-earth simulations for 20 nearby stars

Star	Sp Type	D (pc)	S_*/S_p	S_{EZ}/S_p	SNR
Alp2Cen	K1V	1.3	1507	38	34.1
18Eps Eri	K2V	3.2	269	219	25.2
Eps Ind	K5V	3.6	195	278	22.7
52Tau Cet	G8V	3.6	300	281	20.4
Alp1Cen	G2V	1.3	8313	38	14.7
40Omi2Eri	K1V	5.0	298	537	12.3
82 Eri	G8V	6.1	560	775	8.1
Del Pav	G5IV-Vvar	6.1	657	788	7.7
8Bet CVn	G0V	8.4	524	1480	4.8
44Chi Dra	F7Vvar	8.1	866	1371	4.7
1Pi 3Ori	F6V	8.0	907	1360	4.7
Zet Tuc	F9V	8.6	573	1559	4.5
54Chi1Ori	G0V	8.7	523	1585	4.5
Bet Hyi	G2IV	7.5	1696	1180	4.5
10Alp CMi	F5IV-V	3.5	15367	258	4.1
Gam Pav	F6V	9.2	528	1794	4.0
43Bet Com	G0V	9.2	584	1770	4.0
86Mu Her	G5IV	8.4	1327	1490	4.0
13Gam Lep	F7V	9.0	883	1699	3.9
53Xi UMa	G0 Ve	10.4	756	2291	3.1

these stars and the SNRs for Earths in their habitable zones, along with the star leakage and exo-zodi signal levels, as computed from the simulations for a two-telescope nulling interferometer with a short baseline of 6 m. All other parameters used are the same as those given in Table 1. The SNRs are in the range of 4 to 30 for an integration of 24 hr. These SNRs and signal levels indicate that using a double Bracewell will successfully alleviate the difficulties in separating planet signal and hence will achieve the goals of Earth detections for these stars.

8. CONCLUSION

The simplest IR nulling interferometer, a single Bracewell on a 18 m boom in space, will have the required sensitivity and resolution to survey giant planets in a large sample of young stars and clusters at up to 140 pc. With a modest design change to use it as a double Bracewell, it can detect exo-earths in a sample of 20 nearby stars.

REFERENCES

1. Bracewell R.N., and McPhie R.H., *Icarus*, Vol. 38, 136, 1979.
2. Serabyn E., SPIE 4838, 594, 2003
3. Marcy G.W and Butler R.P., ARA&A, Vol. 37, 54, 1998
4. Burrows A., et al., *ApJ*, Vol. 491, 856, 1997.
5. Pollack J.B., etal. *Icarus*, Vol. 124, 62, 1996.
6. Beichman C.A. and Velusamy T., *Optical and IR Interferometry from Ground and Space*, ASP Conference Ser Vol 194, 405, 1999
7. Shao M., *Ex-NPS Report*, 1996.
8. Woolf N.J., and Angel R.P.J., in *Planets Beyond Solar System and next Generation Space Missions, ASP conference Series*, p285, 1997.
9. Velusamy T., and Beichman C.A., in *2001 IEEE Aerospace Conference* 4-2013, 2001.